Elsevier Editorial System(tm) for Earth and Planetary Science Letters
Manuscript Draft

Manuscript Number: EPSL-D-08-00570

Title: Magnetostratigraphy of the Early Triassic from Chaohu (China) and its implications for the Induan - Olenekian stage boundary

Article Type: Regular Article

Keywords: Chaohu, Lower Triassic, Paleomagnetism, Olenekian, magnetostratigraphy

Corresponding Author: Mr Sun Zhiming, PhD

Corresponding Author's Institution: Institute of Geomechanics, CAGS

First Author: Sun Zhiming

Order of Authors: Sun Zhiming; Mark W. Hounslow; Junling Pei; Laishi Zhao; Jinnan Tong

Abstract: A magnetostratigraphic study was performed on the lower 44 m of the West Pingdingshan section near Chaohu city, (Anhui province, China) in order to provide a magnetic polarity scale for the early Triassic. Data from 295 paleomagnetic samples is integrated with a detailed biostratigraphy and lithostratigraphy. The tilt-corrected mean direction from the West Pingdingshan section, passes the reversal and fold tests. The overall mean direction after tilt correction is D=299.9º, I=18.3º (κ=305.2, α95=1.9, N=19). The inferred paleolatitude of the sampling sites (31.6ºN, 117.8ºE) is about 9.4º, consistent with the stable South China block (SCB), though the declinations indicate some 101o counter-clockwise rotations with respect to the stable SCB since the Early Triassic. Low-field anisotropy of magnetic susceptibility indicates evidence of weak strain. The lower part of the Yinkeng Formation is dominated by reversed polarity, with four normal polarity magnetozones (WP2n to WP5n), with evidence of some thinner (<0.5 m thick) normal magnetozones. The continuous magnetostratigraphy from the Yinkeng Formation, provides additional high-resolution details of the polarity pattern through the later parts of the Induan into the lowest Olenekian. The magnetostratigraphic and biostratigraphic data shows the conodont marker for the base of the Olenekian (first presence of Neospathodus waageni) is shortly prior to the base of normal magnetozone WP5n. This provides a secondary marker for mapping the base of the Olenekian into successions without conodonts.

This section provides the only well-integrated study from a Tethyan section across this boundary, but problems remain in definitively relating this boundary into Boreal sections with magnetostratigraphy.

State Key Laboratory of Geological Processes and Mineral Resources ,
China Universit y of Geosciences, Wuhan, 430074, China

phone: +86-10-68422365, fax: +86-10-68422326

EPSL:
Dear Editor:

Please find enclosed manuscript entitled as "***Magnetostratigraphy of the Early Triassic from Chaohu (China) and its implications for the Induan -Olenekian stage boundary***" by Z. Sun, Mark W. Hounslow, J. Pei et al., we hope you to consider for publish in EPSL.

The names and addresses of my six suggested reviewers are listed as follows:

Robert Scholger,
Institute of Geophysics, University of Leoben, Peter-Tunner-Strasse 25, 8700 Leoben, Austria
scholger@unileoben.ac.at
Giovanni Muttoni
Department of Earth Sciences, University of Milan, via Mangiagalli 34, I-20133 Milan, Italy
Email:giovanni.muttoni1@unimi.it
Yves Gallet
Equipe de Paléomagnétisme, Institut de Physique du Globe de Paris, UMR CNRS 7154, 4 Place Jussieu, 75252 Paris Cedex 05, France
gallet@ipgp.jussieu.fr
Dr. J. Besse
Laboratoire de Paleomagnetisme et Geodynamique, Department de Geomagnetisme et Paleomagnetisme (URA CNRS 729), Institut de Physique de Glove, 4 Place Jussieu, 75252 Paris Cedex 05, France
e-mail: besse@ipgp.jussieu.fr
Dr. Xixi Zhao
Institute of Tectonics and Department of Earth Sciences,
University of California, Santa Cruz
CA 95064, USA
e-mail: xzhao@es.ucs.edu
Michael Szurlies
Institut fur Geologische Wissenschaften, Universitat Halle, DomstraMe 5, 06108 Halle/Saale, Germany
e-mail: szur@gfz-potsdam.de

Thank you very much. I look forward to your reply.

Sincerely yours,
Zhiming Sun

* Manuscript

Magnetostratigraphy of the Early Triassic from Chaohu (China) and its implications for the Induan - Olenekian stage boundary

Zhiming Sun[1], Mark W. Hounslow[2], Junling Pei[3], Laishi Zhao[1], Jinnan Tong[1], James G. Ogg[4]

1. State Key Laboratory of Geological Processes and Mineral Resources , China Universit y of Geosciences, Wuhan, 430074 , China
2. Centre for Environmental Magnetism and Palaeomagnetism, Geography Dept, Farrer Avenue, Lancaster University, Lancaster, UK., LA1 4YQ.
3. Key Laboratory of Crust Deformation and Processes, Institute of Geomechanics, CAGS, Beijing, China
4. Dept. Earth & Atmospheric Science, Purdue University, West Lafayette, IN 47907 USA

Corresponding author:
Zhiming Sun
State Key Laboratory of Geological Processes and Mineral Resources ,
China Universit y of Geosciences,
Wuhan, 430074
China
phone: +86-10-68422365, fax: +86-10-68422326
e-mail: sunzm1209@yahoo.com.cn

Abstract

A magnetostratigraphic study was performed on the lower 44 m of the West Pingdingshan section near Chaohu city, (Anhui province, China) in order to provide a magnetic polarity scale for the early Triassic. Data from 295 paleomagnetic samples is integrated with a detailed biostratigraphy and lithostratigraphy. The tilt-corrected mean direction from the West Pingdingshan section, passes the reversal and fold tests. The overall mean direction after tilt correction is D=299.9º, I=18.3º (κ=305.2, α95=1.9, N=19). The inferred paleolatitude of the sampling sites (31.6ºN, 117.8ºE) is about 9.4º, consistent with the stable South China block (SCB), though the declinations indicate some 101^{o} counter-clockwise rotations with respect to the stable SCB since the Early Triassic. Low-field anisotropy of magnetic susceptibility indicates evidence of weak strain. The lower part of the Yinkeng Formation is dominated by reversed polarity, with four normal polarity magnetozones (WP2n to WP5n), with evidence of some thinner (<0.5 m thick) normal magnetozones. The continuous magnetostratigraphy from the Yinkeng Formation, provides additional high-resolution details of the polarity pattern through the later parts of the Induan into the lowest Olenekian. The magnetostratigraphic and biostratigraphic data shows the conodont marker for the base of the Olenekian (first presence of *Neospathodus waageni*) is shortly prior to the base of normal magnetozone WP5n. This provides a secondary marker for mapping the base of the Olenekian into successions without conodonts. This section provides the only well-integrated study from a Tethyan section across this boundary, but problems remain in definitively relating this boundary into Boreal sections with magnetostratigraphy.

Key words: Chaohu, Lower Triassic, Paleomagnetism, Olenekian, magnetostratigraphy

1. Introduction

Magnetostratigraphy can be used as an essential tool for chronostratigraphic correlations between rocks from different environments including those that are unfossiliferous or have poor fossil preservation. The Lower Triassic magnetostratigraphy has been studied in many places, where progress has been made in constructing a magnetic polarity scale for the Permian-Triassic boundary interval either from marine (Heller et al., 1988,1995; Haag et al., 1991; Li et al., 1989; Steiner et al., 1989; Chen et al., 1994; Embleton et al., 1996; Zhu et al., 1999; Scholger et al., 2000; Gallet et al., 2000; Hounslow et al., 2008) or terrestrial rocks (Molostovsky, 1996; Szurlies et al., 2003; Steiner, 2006; Szurlies, 2007). In spite of this, discussions continue about how to precisely correlate marine and continental facies using magnetostratigraphy near the Permian-Triassic boundary (PTB) interval and the remainder of the Lower Triassic (Steiner, 2006; Szurlies, 2007; Hounslow et al., 2008). This in part reflects the debate about the placement of the base of the 2nd stage of the Triassic, the Olenekian, as well as differing quality, quantity and types of secondary biostratigraphic constraints in these Early Triassic successions. In addition, paleomagnetic studies from some continuous marine sections have differing magnetostratigraphic records (e.g. the Induan global stratotype section and point (GSSP) at Meishan; Yin et al. 2005) perhaps because of undetected remagnetization (Li et al., 1989; Zhu et al., 1999; Steiner, 2006).

Recent investigations were carried out on the west Pingdingshan section to provide detailed biostratigraphic and lithostratigraphic information for the Induan–Olenekian boundary (Tong et al; 2003, 2005, 2007; Zhao et al., 2007, 2008). Based on this robust lithostratigraphic and biostratigraphic framework, a precise positioning of paleomagnetic data was achieved, resulting in a detailed composite magnetic record. Along with biostratigraphic data, the magnetic record of these lowermost Triassic sediments are important in that they provide an integrated magnetostratigraphic and biostratigraphic reappraisal that allows the recognition of the Induan– Olenekian boundary in a Tethyan section. This is all the more important, in that the ratified GSSP for the Olenekian at Mud (Spiti, India) is unlikely to ever have a magnetostratigraphy because of low grade metamorphism (Krystyn et al., 2007)

2. Geological setting

The West Pingdingshan section (location 31.6ºN, 117.8ºE), located near Chaohu city, Anhui province, China, consists of interbedded calcareous mudstones and limestones. The section is one of the well-exposed Lower Triassic successions in

South China (Fig. 1), which was deposited in a carbonate ramp setting on the Lower Yangtze Block, within the low-latitude eastern Tethyan archipelago. The Lower Triassic sections near Chaohu city have been extensively investigated using a variety of detailed lithostratigraphic, biostratigraphic and chemostratigraphic tools (Tong et al., 2003, 2005, 2007; Zhao et al., 2007, 2008). The Lower Triassic succession at Chaohu yields abundant fossils, which provides a comprehensive biostratigraphy marked by conodonts and ammonoids (Fig. 2).

Information is presented on a set of palaeomagnetic samples collected from the lower 44 m of the West Pingdingshan section, from the latest Permian into the Olenekian. The latest Permian ammonoids occur in the highest beds of the Dalong Formation just 11.5 cm below the "boundary clay bed". Beds containing *Claraia* and *Ophiceras* occur about 50 cm above the "boundary clay bed", which is located at 0.33 m in the section. More extensive biostratigraphic data on the overlying Induan is summarized in Zhao et al. (2007). The conodont specimens from the West Pingdingshan section are not clearly darkened and have a conodont alteration index of about 2.0, which is consistent with alteration index's of 1.5 to 2.0 in the general study region (Wang, 1993). The bedding in the West Pingdingshan section dips at some 78-88^{o} towards the E, forming part of the core of the Majiashan-Pingdingshan synclinorium.

3. Sampling and paleomagnetic procedures

A total of 347 drill-plugs were collected for palaeomagnetic investigations from the Yinkeng Formation. These were collected, using a gasoline-powered drill, and were oriented using a magnetic compass. Samples were collected at 10-15 cm intervals. The sampling interval covers the stratigraphic interval from just below the lithologic PTB (at 0. 33m), to just above the base of the Olenekian (at first occurrence (FO) of *Neospathodus waageni eowaaageni,* morphotype of *Ns. waageni*).

Fifty-two drill-plugs did not produce suitable paleomagnetic specimens for the magnetometer. The suitable remaining 295 specimens underwent stepwise thermal demagnetization using 15-20 steps in an ASC TD-48 oven with an internal residual field less than 10nT. Remanent magnetization was measured with a 2G cryogenic magnetometer at the palaeomagnetic laboratory of the Institute of Geomechanics, CAGS in Beijing. The magnetometer is located inside a Helmholtz coils that reduces the ambient geomagnetic field to around 300nT. Remanent component directions were determined by principal component analysis, as implemented in the Enkin suite of software. The software of Cogné (2003) and Kent et al (1983) was used in the analysis of the resulting demagnetisation data. A KLY-4 Kappabridge susceptibility system was used to measure the anisotropy of magnetic susceptibility (AMS) of 137 specimens, prior to thermal demagnetisation, to assess if these rocks have suffered substantive tectonic strain. The magnetic mineralogy of representative lithologies was studied using stepwise thermal demagnetization (Lowrie, 1990) of isothermal remanent magnetization (IRM). The IRM was imparted using an ASC scientific pulse magnetizer (Model IM-10-30). Thermal demagnetization of the three-component IRM used fields of 0.12 T, 0.4 T and 1.2 T.

4. Magnetic mineralogy results

The anisotropy degree (P') of the samples ranges from 1.001 to 1.057 (Fig. 3a). The mean anisotropy degree is 1.013. The anisotropy shape factor (T) varies widely, mostly independent of P', and is distributed mostly in the oblate field (T >0; Fig. 3a). The principal anisotropy directions (K1) are dispersed but show some evidence of a preferred N-S orientation (Fig. 3b). The K3 directions are on average perpendicular to the bedding plane. The low degree of anisotropy and the reasonably large scatter in the maximum susceptibility axis directions within the bedding plane, indicates these rocks have not experienced large amounts of tectonic strain, although the orientation of the K1 axes approximately parallel to the Majiashan-Pingdingshan synclinorium axis is evidence of weak strain, not out of the ordinary for such gently folded rocks.

Thermal demagnetization of the soft (<0.12 T) and medium (0.12-0.4 T) fractions shows an unblocking temperature of 560-580°C, indicative of magnetite. The hard fraction (0.4-2.7 T) shows a distinct unblocking temperature between 630-660°C, which is probably indicative of hematite (Fig. 4).

5. Palaeomagnetic Results

The specimens have initial natural remanent magnetisation (NRM) intensities between 10^{-4} and 10^{-3} A/m. Thermal demagnetization isolated three magnetisation components:

(a) Firstly a low-temperature component (component A: LTC) is isolated in all samples below about 300°C. The mean direction of this component before tilt correction is D=3.0°, I=41.5° (N=295 and α_{95}=1.3°), and is similar to the present-day field direction (D=355.4° and I= 47.3°; Fig. 5a, 6), which is inferred to be the origin of this component.

(b) A second component (component B: MTC) is determined mostly between the 300-480°C demagnetisation steps, by a well-defined linear segment on the orthogonal vector diagrams in nearly all specimens. This magnetisation component largely dominates the NRM. This component is NNW and down-directed in geographic coordinates and easterly and down-directed in stratigraphic coordinates (Fig. 5b, 6). The Fisher precision parameter of the mean direction of the MTC component changes from 42.2 before bedding correction to 40.3 after bedding correction, indicating a slightly tighter directional dispersion in situ coordinates (Fig. 5b). The mean magnetization direction at 350°, +32° (k=42.2, α_{95}= 1.4) in geographic coordinates is not distinct from that expected for the Jurassic-Cretaceous of the South China block (SCB). Hence, we interpret this component B as probably a remagnetization acquired during the Jurassic-Cretaceous period, after tilting of the beds.

(c) Thirdly a high-temperature component (component C: HTC). This component is mostly present between 480-580°C. Its direction is of dual polarity, and is interpreted as a Triassic magnetisation (Fig. 6, 8). Only some 66% of samples showed evidence of this magnetisation component, the remaining specimens were dominated by component B until complete demagnetisation. Component C has a strong overlap of unblocking temperature with component B in a large majority of specimens at and above 480°C. Only some 11% of specimens show clear linear segments, separating component C from component B on Zijderveld plots and principle component (PCA) analysis (Fig. 6, 7).

Categories of demagnetisation behavior were visually assigned (assisted by the PCA analysis) to several classes of demagnetization data shown by the specimens.

Firstly, a category indicating no component C could reliably be interpreted from the specimen data (‘MTC only’ in Fig. 9). This type of behaviour is dominant in the lower 5 m of the section (which is more weathered than the overlying parts), and above 20 m in the section (Fig. 7). Some 34% of specimens possess this type of behavior.

Secondly, two classes (good and poor) of ChRM line-fit data (Fig. 6, 9), which are exclusively present in the levels between 5 and 30 m (Fig. 9). Some 11% of samples possess this type of behavior.

Thirdly, specimen data, which showed evidence of incomplete separation of components B and C, but which showed evidence of great circle trends towards either the reverse or normal polarity directions of component C (‘GC trends’ in Fig. 9). Two sub-categories of good and poor behavior were evaluated, based on the amount of approach towards the component C dual polarity directions (Fig. 8, 9). Some 55% of specimens possess this type of behavior. Great circles were predominantly fitted through the higher temperature demagnetisation steps as an estimate of these great circle trends.

The reversal test (McFadden & McElhinney, 1990) has been performed on the component C mean direction. The test indicates a positive reversal test (Ra), with less than 5° degrees between inverted antipodal mean directions (γ_{Obs}=2.3; $\gamma_{Critical}$=4.4). The tilt test on the site-mean directions of ChRM is also positive at the 95% level of confidence according to the criteria of McFadden and Jones (1990) (Xi_2Is=6.8, Xi_2Tc=1.8, Critical 95%=5.07). These findings indicate the primary nature of the ChRM from the West Pingdingshan section. The site-mean directions were determined using the combined ChRM line-fit and fitted great circle data using the method of Mcfadden and McElhinny (1988), as implemented in the Cogné (2003) software (Fig. 8). The averaged site-mean direction for component C is D_g=285.1°, I_g=-62.7°, κ_g=193.7, α_{95}=2.4° before tilt correction, and D_s=299.9°, I_s=18.3°, κ_s=305.2, α_{95}=1.9°, N=19 after tilt correction (Fig. 8a, Table 1). The average direction of each group of sites was calculated using the great circles (re-magnetisation circles) /fixed points to evaluate one of the means displayed in Fig. 8a, for example the samples in bed AC14 (Fig. 8b). The determined paleopole lies at 30.3°N, 19.9°E with A_{95}=1.4° (dp/dm=1.0/2.0). The paleolatitude of 9.4° for the section is not significantly different (at 95% confidence level) with that predicted for the stable South China Block (Heller et al., 1988, 1995; Steiner et al., 1989). Hence, we infer component C is a Lower Triassic magnetisation, acquired prior to folding. However, the mean directions for the ChRM are substantially different in declination from the Lower Triassic means for the South China block, a result of 101.2° (±3.3°) anti-clockwise vertical axis rotation with respect to the stable South China block. Similar anticlockwise rotations occur further south adjacent to the Tanlu fault (Tan et al., 2007). These are probably associated with local rotation of the Chaohu area, during docking with the nearby North China block, along the Tanlu fault.

6. *Magnetostratigraphy and global magnetostratigraphic correlation*

The ChRM directions were converted to VGP latitude (displayed as filled circle in Fig. 9). For those specimens possessing great-circle behaviour, the point on the fitted great circle closest to the section mean direction was used to calculate the VGP latitude (displayed as open circle in Fig. 9). The magnetic polarity of the section is dominated by reverse polarity, with three normal polarity magnetozones represented by three or more specimens (WP2n, WP3n and WP4n). Normal magnetozones WP1r.1n and WP5n are defined by only two specimens. A number of tentative normal polarity sub-magnetozones, represented by a single specimen are also present within WP4r, with only that in bed 19 defined by PCA line-fit data (Fig. 9).

The magnetic polarity at the correlated base of the Olenekian (at the first occurrence of morphotype *Ns. waageni eowaggeni* in subbed 24-16) is probably reversed, since underlying sub-bed 24-15 and overlying sub-bed 24-17 are reversed, with both sampled intervening beds not containing any evidence of Triassic component C. The base of the overlying normal magnetozone W5n is ~2.5 m above the FA of *Ns. waageni eowaggeni,* although a substantial number of specimens in the base of bed 25 posses no component C. Hence, the base of magnetozone WP5n provides a good secondary marker a little above the base of the Olenekian in the West Pingdingshan section.

The dominance of reverse polarity in the lower part of the section (i.e. that below bed 15, Figs. 9 & 10) would suggest, according to the magnetostratigraphy, that this interval is entirely late Griesbachian, since no substantive evidence of the equivalent of normal polarity magnetozone LT1n, which characterizes the basal Induan, occurs in the base of the section (Fig. 10). It is perhaps possible the normal magnetozone WP1r.1n, some 2.0 m above the "PTB set" (Peng et al., 2001), may represent part of LT1n and the remainder of the basal Griesbachian normal magnetozone is obscured by the scarcity of polarity data in this interval (Fig. 9). The basal part of the West Pingdingshan section was only uncovered in recent years, and not much biostratigraphic work has been done on it, but neighboring sections such as the north Pingdingshan and west Majiashan sections have been studied in detail at the boundary, with no evident breaks in sedimentation.

The magnetostratigraphy of the Gaundao section is ambiguous around the Induan-Olenekian boundary (IOB), but the positive carbon isotopic excursion allows approximate correlation from Gaundao to the West Pingdingshan and Bulla/Suisi sections (Payne et al. 2004; Horacek et al. 2007; Tong et al. 2007; Richoz et al. 2007; Fig. 10). The magnetostratigraphy of the upperpart of the West Pingdingshan section, has a close correspondence in polarity style to that at Hechuan, as does the reverse-polarity dominated interval at Guandao, which covers the upper range of the conodont *Ns. dieneri* (Fig. 10). The most complete magnetostratigraphy across the IOB occurs in the Boreal realm from the Sverdrup Basin in Canada and Spitsbergen in arctic Norway (Ogg & Steiner, 1991; Hounslow et al., 2008). However, correlation of the IOB onto the magnetostratigraphy of the boreal sections is problematic with two possible solutions.

Both *Ns. kummeli*, *Ns. dieneri* and *Ns. svalbardensis* are known from the *P. candidus* Zone in Canada (Orchard & Tozer, 1997), which suggests the reverse polarity interval covering beds 18-20 at West Pingdingshan (Fig. 10) represents the lower part of magnetozone LT2r (GC2r at Griesbach Creek; Sc2r at Creek of Embry and Vh4r at Vikinghøgda; Fig. 10) in the Boreal composite magnetic polarity timescale (MPTS). *Ns. dieneri* and *Ns. cristagalli* are present in the Canadian *V. sverdrupi* Zone (Orchard & Tozer, 1997) and in sections on Spitsbergen *V. spitzbergensis* (probable synonym of *V. sverdrupi*) occurs with *Ns. pakistanensis*, *Ns. dieneri*, and *Ns.* aff. *svalbardensis* (Nakrem et al., in-review), which suggests the boundary between the *Ns. cristagalli* and *Ns. pakinstanensis* conodont zones at the GSSP in Mud (Krystyn et al. 2007), occurs within the Boreal Sverdrupi Zone. Within Canadian sections *Ns. waageni* first occurs within the *Euflemingites romunderi* Zone, whereas in Siberian sections *Ns. waageni* first occurs some 20% through the *H. hedenstroemia* Zone (Dagis, 1984), indicating that the IOB probably occurs within the lower part of the *H. hedenstroemi* Zone. This suggests that the magnetozone WP5n at West Pingdingshan is probably the equivalent of magnetozone LT4n in the boreal MPTS (option ① in Fig. 10), and hence the IOB is within the uppermost part of LT3r. A consequence of this biostratigraphic-driven correlation is that the equivalent of LT3n in the MPTS appears to be unconvincingly detected at West Pingdingshan- possibly represented by WP4n in bed 19? (Fig. 10).

A second, lower placement of the IOB, relative to the magnetostratigraphy is also possible (Option ② in Fig. 10). Since the ammonoid control at Griesbach Creek is based on spot occurrences, its not clear where the base of the *H. hedenstroemi* Zone is located, its may be that it is located below the base of the Smith Creek Member in the upper part of GC2r (Fig. 10). Consequently, it is possible that WP5n is the equivalent of GC3n (LT3n in MPTS). Two features support this possibility; firstly, this correlation is more consistent with the magnetostratigraphy, in that no substantive normal magnetozone is detected in beds 18 to 24 at West Pingdingshan. Secondly, at both the Griesbach Creek and Vikinghøgda sections close to the lower boundary of GC3n and Vh5n (LT3n in MPTS) is a major transgressive surface, which may be the equivalent of that seen at Chaohu and Mud close to the IOB (Guo et al., 2007; Krystyn et al 2007).

With these uncertainties in correlation of marine sections in mind, its premature to attempt mapping of the cyclo-magnetostratigraphy from the Buntsandstein (Szurlies, 2007) into the marine sections. In addition much reliance has been placed on relating the Italian sections at Bulla and Siusi (Scholger et al., 2000) to age-calibrate the Buntsandstein cycles and lithostratigraphy (Szurlies et al., 2003; Szurlies 2007), yet the isotopic curves from these Italian sections clearly located the IOB higher in the Bulla/ Siusi sections than that used by Szurlies (2007).

7. Conclusion

A dual polarity Triassic magnetisation can be extracted from the West Pingdingshan section, in spite of minor associated tectonic deformation, and partial remagnetisation. The Early Triassic magnetization is masked by a strong Jurassic-Cretaceous overprint magnetization, acquired post-tilting, which variably masks the Early Triassic magnetisation. Nevertheless some 66% of specimens display evidence in the demagnetisation diagrams of characteristic polarity, either through conventional magnetisation component isolation, or great circle trends. The correlated conodont marker for the base of the IOB in the GSSP at Mud (FA of *Ns. dieneri s.l.*) indicates that at West Pingdingshan the IOB is some 2.5 m below a normal magnetozone, which provides a secondary marker, for mapping the base of the Olenekian into successions without conodonts. Around the IOB the West Pingdingshan section can be correlated confidently to other Tethyan Lower Triassic successions, but which however lack the corroborative magnetostratigraphic details shown at Chaohu. Problems remain near the Permian-Triassic boundary in the West Pingdingshan section, due to inadequate recovery of Triassic magnetisations from specimens. Problems also remain in relating the Induan-Olenekian boundary interval into the boreal sections in Canada and Spitsbergen with magnetostratigraphy.

Acknowledgements

This study was supported by NSFC (40102021), Leo Krystyn provided useful discussion on biostratigraphic correlations.

.

References

Chen, H., Sun, S., Li, J., Heller, F., Dobson, J., 1994. Magnetostratigraphy of the Permian and Triassic in Wulong, Sichuan Province, Science in China B 12, 1317-1324.

Cogné, J. P., 2003. PaleoMac: A Macintosh™ application for treating paleomagnetic data and making plate reconstructions. Geochemistry Geophysics Geosystems 4, doi:10.1029/2001GC000227.

Dagis, A.S., 1984. Early Triassic conodonts of the north Middle Siberia. Nauka, Moscow, 69 p. (in Russian).

Embleton, B. J. J., McElhinny, M.W., Ma, X., Zhang, Z., Li, Z., 1996. Permo-Triassic magnetostratigraphy in China: the type section near Taiyuan, Shanxi Province, North China, Geophys Journal International 126, 382-388 Scopus.

Gallet, Y., Krystyn, L., Besse, J., Saidi, A., and Ricou, L-E., 2000. New constraints on the upper Permian and Lower Triassic geomagnetic polarity timescale from the Abadeh section (central Iran): Journal Geophysical Research 105, 2805-2815 Scopus.

Guo, G., Tong, J., Zhang, S., Zhang, J., Bai, L., 2007. A study on the Lower Triassic cyclostratigraphy in the West Pingdingshan Section, Chaohu, Anhui Province. Science in China (Series D) 37, 1571-1578.

Haag, M., Heller, F., 1991. Late Permian to Early Triassic magnetostratigraphy, Earth and Planetary Science Letters 107, 42-54 Scopus.

Heller, F., Chen, H., Dobson, J., and Haag, M., 1995. Permian- Triassic magnetostratigraphy - new results from south China: Physics Earth Planetary Interiors 89, 281-295 Scopus.

Heller, F., Lowrie, W., Li, H., Wang, J., 1998. Magnetostratigraphy of the Permo-Triassic boundary section at Shangsi (Guangyuan, Sichuan Province, China), Earth and Planetary Science Letters 88, 348-356 Scopus.

Horacek, M., Brandner, R. & Abart, R., 2007. Carbon isotope record of the P/T boundary and the Lower Triassic in the Southern Alps: Evidence for rapid changes in storage of organic carbon. Palaoegeography, Palaeoclimatology, Palaeoecology 252, 347-354 Scopus.

Hounslow, M.W. Peters, C. Mørk, A. Weitschat, W. & Vigran, J.O. 2008. Bio-magnetostratigraphy of the Vikinghøgda Formation, Svalbard (arctic Norway) and the geomagnetic polarity timescale for the Lower Triassic. Bull. Geol. Soc. America. In press.

Kent, J.T., Briden, J.C. & Mardia, K.V. 1983. Linear and planar structure in ordered mulivariate data as applied to progressive demagnetization of palaeomagnetic remanance. Geophysical Journal of the Royal Astronomical Society 81, 75–87 Scopus.

Krystyn, L., Bhargava, O.N. Richoz, S., 2007. A candidate GSSP for the base of the Olenekian Stage: Mud at Pin Valley; district Lahul & Spiti, Hamachal Pradesh (Western Himalaya), India. Albertiana 35, 5-29.

Lehrmann, D.J., Ramezani, J., Bowring, S.A., Martin, M.W., Montogomery, P., Enos, P., Payne, P., Orchard, M.J., Wang, H., and Wei, J., 2006. Timing and recovery from the end Permian extinction: geochronologic and biostratigraphic constraints from south China: Geology 34, 1054-1056.

Li, H., Wang, Z., 1989. Magnetostratigraphy of Permo-Triassic boundary section of Meishan of Changxing, Zhejiang, Science in China (Series D) 32, 1401-1408.

Lowrie, W., 1990. Indentification of ferromagnetic minerals in a rock by coercivity and unblocking temperature properties, Geophysical Research Letter 17, 159-162 Scopus.

McFadden, P. L., 1990. A new fold test for palaeomagnetic studies. Geophysical Journal International 103, 163-169 Scopus.

McFadden, P.L., and McElhinney, M.W., 1988. The combined analysis of remagnetisation circles and direct observations in paleomagnetism. Earth and Planetary Science Letters 87, 161-172.

McFadden, P.L., and McElhinny, M.W., 1990. Classification of the reversal test in paleomagnetism: Geophysical Journal International 103, 725-729 Scopus.

Molostovsky, E.A. 1996. Some aspects of magnetostratigraphic correlation. Stratigraphy and Geological correlation 4, 231-237 Scopus.

Ogg, J.G., and Steiner, M.B., 1991. Early Triassic polarity time-scale: integration of magnetostratigraphy, ammonite zonation and sequence stratigraphy from stratotype sections (Canadian Arctic Archipelago): Earth and Planetary Science Letters 107, 69-89.

Orchard, M.J. & Tozer, E.T. 1997. Triassic conodont biochronology, its calibration with the ammonoid standard and a biostratigraphic summary for the western Canada sedimentary basin. Bulletin of Canadian Petroleum Geology 45, 675–692 Scopus.

Payne, J. L., Lehrmann, D. J., Wei, J., Orchard, M. J., Schrag, D. P., Knoll, A. H., 2004. Large perturbations of the carbon cycle during recovery from the end-Permian extinction. Science 305, 506-509 Scopus.

Peng, Y., Tong J., Shi, G.R., and Hansen, H.J., 2001. The Permian-Triassic boundary stratigraphic set: characteristics and correlation. Newsletter on Stratigraphy 39, 55–71 Scopus.

Perri, M.C., and Farabegoli, E., 2003. Conodonts across the Permian-Triassic boundary in the southern Alps: Courier Forschungsinstitut Senckenberg 245, 281-313.

Richoz, S. Krystyn, L., Horacek, M., & Spötl, C. 2007. Carbon isotope record of the Induan –Olenekian candididate GSSP Mud and comparison with other sections. Albertiana 35, 35-39.

Scholger, R., Mauritsch, H.J., and Brandner, R., 2000. Permian-Triassic boundary magnetostratigraphy from the southern Alps (Italy): Earth and Planetary Science Letters 176, 495-508 Scopus.

Steiner, M. 2006. The magnetic polarity timescale across the Permian-Triassic boundary, *in* Lucas, S.G. Cassinis, G. and Schneider, J.W., eds., Non-marine Permian biostratigraphy and biochronology: Geological Society, London Special Publication, 265, 15-38.

Steiner, M., Ogg, J., Zhang, Z., and Sun, S., 1989. The Late Permian/early Triassic magnetic polarity time scale and plate motions of south China: Journal Geophysical Research 94, 7343-7363 Scopus.

Szurlies, M. Bachmann, G. H. Menning, M. Nowaczyk, N.R. Käding, K.-C. 2003. Magnetostratigraphy and high resolution lithostratigraphy of the Permian- Triassic boundary interval in Central Germany. Earth and Planetary Science Letters 212, 263-278 Scopus.

Szurlies, M. 2007. Latest Permian to Middle Triassic cyclo-magnetostratigraphy from the Central European Basin, Germany: Implications for the geomagnetic polarity timescale. Earth and Planetary Science Letters 261, 602-619 Scopus.

Tan, X, Kodama, K.P., Gilder, S., Courtillot, V., Cogn’e, J.P., 2007. Palaeomagnetic evidence and tectonic origin of clockwise rotations in the Yangtze fold belt, South China Block. Geophysical Journal International 168, 48–58 Scopus.

Tong, J., Hansen, H. J., Zhao, L., and Zuo, J., 2005. High resolution Induan- Olenekian boundary sequence in Chaohu, Anhui Province: Science in China (Series D) 48, 291-297 Scopus.

Tong, J., Zakharov, Y. D., Orchard, M. J., Yin, H., and Hansen, H. J., 2003. A candidate of the Induan-Olenekian boundary stratotype in the Tethyan region. Science in China (Series D) 46, 1182-1200 Scopus.

Tong, J., Zuo J. & Chen Z.Q. 2007. Early Triassic carbon isotope excursions from South China: Proxies for devastation and restoration of marine ecosystems following the end-Permian mass extinction. Geological Journal 42, 371–389 Scopus.

Wang, C., Conodonts of the Lower Yangtze Valley. 1993. An Index to Biostratigraphy and Organic Metamorphic Maturity. Science Press, Beijing (In Chinese with English summary).

Yin, H., Tong J. and Zhang K., 2005. A review on the Global Stratotype Section and Point of the Permian-Triassic Boundary. Acta Geologica Sinica 79, 715-728

Yin, H., Zhang, K., Tong, J., Yang, Z., and Wu, S., 2001. The Global Stratotype Section and Point (GSSP) of the Permian-Triassic Boundary: Episodes 24, 102-114 Scopus.

Zhao, L., Orchard, M.J., Tong, J., Sun, Z., Zuo, J., Zhang, S., Yun, A. 2007. Lower Triassic conodont sequence in Chaohu, Anhui Province, China and its global correlation. Palaoegeography, Palaeoclimatology, Palaeoecology 252, 24-38 Scopus.

Zhao, L., Tong, J., Sun, Z., Orchard, M., 2008. A detailed Lower Triassic conodont biostratigraphy and its implications for the GSSP candidate of the Induan–Olenekian boundary in Chaohu, Anhui Province. Progress in Natural Science 18, 79–90 Scopus.

Zhu, Y. & Lui, Y., Magnetostratigraphy of the Permian- Triassic boundary section at Meishan, Chanxing, Zheijiang Province, *in* Yin, H. & Tong, J., eds., 1999. Pangea and the Paleozoic-Mesozoic transition: China University of Geosciences Press, Wuhan, 79-84.

Figure captions:

Fig. 1 (a) simplified geological map of Chaohu area and (b) Geographic location.

Fig. 2 Vertical range and zonation of conodonts, ammonoids and bivalves assemblage at West Pingdingshan section, Chaohu, Anhui Province. Modified after Zhao et al. (2008). Bold lines highlight the occurrence of the most important ammonoids and conodonts used to identify the Induan-Olenekian boundary.

Fig. 3(a) Anisotropy of magnetic susceptibility (AMS) plots of shape parameter T versus anisotropy degree P', (b) stereographic projection of AMS principle axes in stratigraphic coordinates for specimens from the Yinkeng Fm. K1 (square): maximum axis, K3 (circle): minimum axis, K2 (triangle): intermediate axis.

Fig. 4 Representative plots of thermal demagnetisation of 3-axis isothermal remanent magnetization, using magnetizing fields of 0.12 T (soft), 0.4 T (medium) and 2.7 T (hard). these plots show Tc at ~ 560-580 and 630-660.

Fig. 5 (a) Equal-area projections of a) the low temperature (LTC or A) component and b) the mid temperature (MTC or B) component. Star is the geocentric axial dipole field, and square the present-day field directions.

Fig. 6 Representative orthogonal demagnetization diagrams (in stratigraphic coordinates). The characteristic magnetisation (component C) directions in the specimens displayed were determined by principle component line-fits. a-e: good quality line-fit from 480 °C through the origin; f-i: poor quality line-fit from 480 °C through the origin; (d), (e), (i): Normal polarity; (a)-(c), (f)-(h): Reverse polarity. Demagnetization steps in °C in all plots.

Fig. 7 Equal-area projections of the magnetisation directional tracks during thermal demagentization of representative samples with a variable content of component C (all in stratigraphic coordinates). G1: good quality great circle data; G2: poor quality great circle (with only short paths towards directions that are consistent with component C being present). Plot c) is for a normal polarity sample, all others for interpreted reverse polarity specimens. In general, these specimen show motion along a great-circle paths in a southeasterly direction, trending towards negative inclination or a northwesterly direction with a postive inclination. The great-circle path is best defined from about 480 °C to 580 °C.

Fig. 8 (a) Equal-area stereographic projection of mean directions of high temperature component C for stratigraphic groups of specimen data. Lower (upper) hemisphere directions are marked with closed (open) symbols. (b) Equal-area stereographic projection of the site (AC14) showing the great circles (re-magnetisation circles) /fixed points used to evaluate one of the means displayed in Fig. 8a. Ellipses are 95% confidence cones of group means. Stars=mean directions of these dual polarity magnetisations.

Fig. 9 Demagnetisation behaviour (see text), virtual geomagnetic pole (VGP) latitude, and the magnetic polarity interpreted in the West Pingdingshan section, along with summary biostratigraphic data (Zhao et al., 2007). Magnetozones defined by no adjacent specimens of the same polarity, are indicated by half bars, with full bars indicating two or more adjacent specimens of the same polarity. Full grey bars indicate adjacent specimens with only component B present. The major N-R magnetozone couplets have been labeled WP (for West Pingdingshan), for ease of description.

Fig. 10 Comparison of the magnetostratigraphy at Chaohu with other studies of marine sections through the latest Permian and Lower Triassic. Data for polarity columns: Guandao (Lehrmann et al., 2006), Hechuan (Steiner et al., 1989), Abadeh (Gallet et al., 2000), Bulla/Siusi (Scholger et al., 2000; Perri & Farabegoli, 2003; Horacek et al., 2007). Griesbach Creek, Smith Creek and Creek of Embry (Ogg & Steiner, 1991 modified by Hounslow et al 2008), Vikinghøgda and composite magnetic polarity timescale (MPTS) from Hounslow et al. (2008).

Table 1

Site-mean paleomagnetic results from the West Pingdingshan section at Chaohu, Anhui Province.

Bed/Site	n	D_g (°)	I_g(°)	D_s(°)	I_s(°)	κ	α95(°)
ac24	9	107.3	67	124.7	-17.1	30.9	5.4
ac23	11	106	63.9	122.5	-19.5	42.5	4.6
ac22	12	100.3	62.9	117.9	-19.8	23.5	5.6
ac21	8	107.8	67.2	121.8	-17.9	13.3	8.4
ac20	7	116.2	63.9	124.8	-19.2	24.9	7.9
ac19	10	303.5	-61.6	308.2	20	28.5	5
ac18	12	114	62.4	123.3	-19.2	22.2	5.2
ac17	9	267.9	-66	294.4	14.5	14.7	7.5
ac16a	7	278.1	-70.7	300.3	14.1	16.7	9.7
ac16b	7	292.8	-61.8	301.6	24.7	8.3	15.3
ac15	11	100	62.5	116.2	-21.4	10.5	9.8
ac14	14	94.6	62	115.9	-17.5	50.6	3.4
ac13	11	96.6	61.7	117.7	-16.8	25.3	5.6
ac12	10	91.7	58.2	113.3	-17.5	39.6	4.2
ac11	7	98.2	62.8	119	-16.4	28.5	6.4
ac10	10	107.6	54.7	116.8	-20.4	20.8	6.4
ac9	10	109.3	55.3	118	-20.3	30.8	4.8
ac8	10	103.9	60.3	117.5	-14.5	13.4	7.9
ac7	10	297.8	-59.9	304.1	16.4	12.3	7.8
mean	19	285.1	-62.7	-	-	193.7	2.4
		-	-	299.9	18.3	305.2	1.9

n: number of specimens used to calculate mean; D_g, I_g, D_s, I_s: declination and inclination in geographic and stratigraphic coordinates respectively; κ: the best estimate of the Fisher precision parameter; α95: the radius of the 95% cone of confidence.

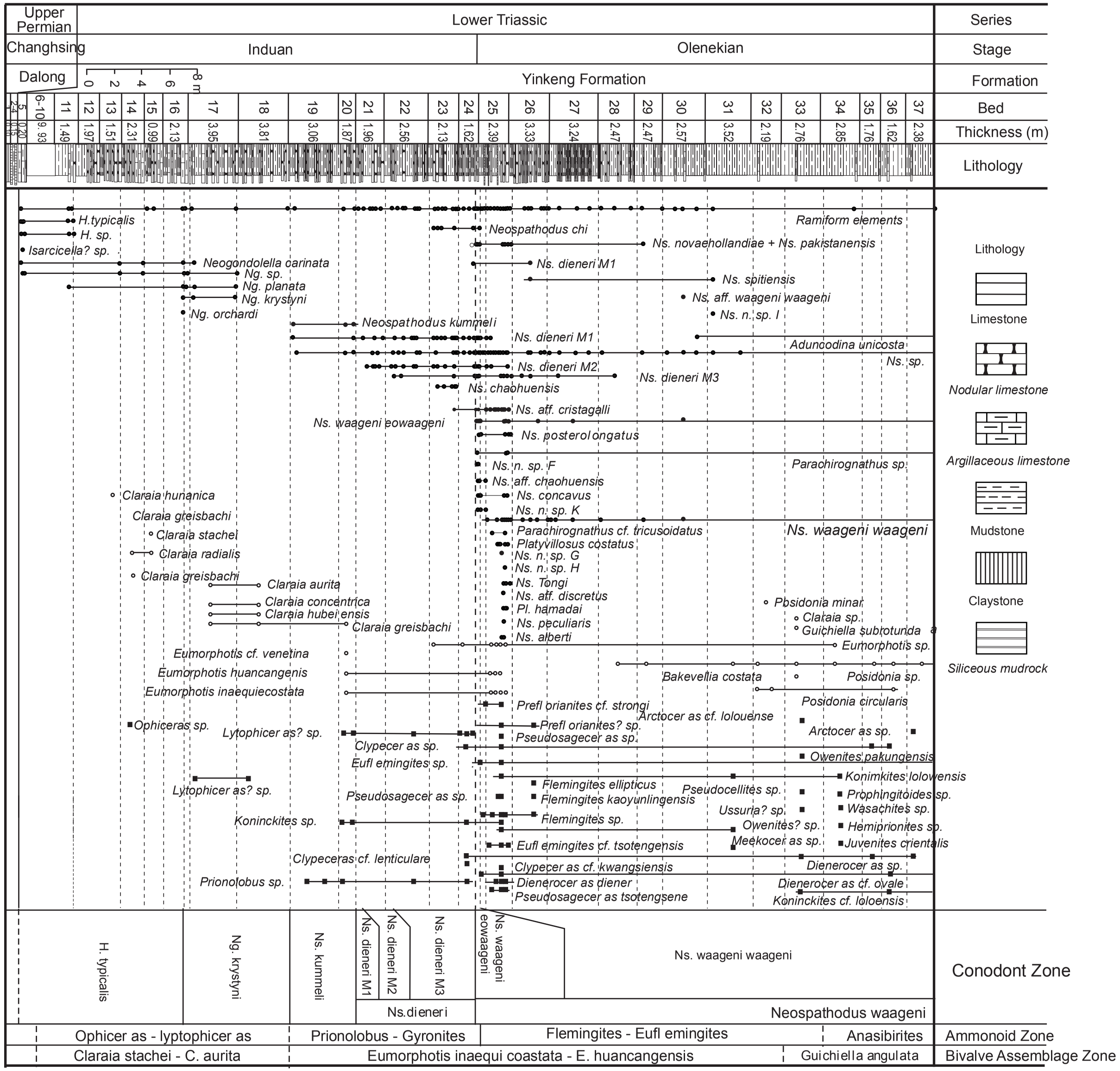

Series
Stage
Formation
Bed
Thickness (m)
Lithology
Upper Permian
Lower Triassic
Changhsing
Induan
Olenekian
Dalong
Yinkeng Formation
0 2 4 6 8 m
Ramiform elements
H.typicalis
H. sp.
Isarcicella? sp.
Neospathodus chi
Ns. novaehollandiae + Ns. pakistanensis
Ns. dieneri M1
Ns. spitiensis
Ns. aff. waageni waageni
Ns. n. sp. I
Neogondolella carinata
Ng. sp.
Ng. planata
Ng. krystyni
Ng. orchardi
Neospathodus kummeli
Aduncodina unicosta
Ns. sp.
Ns. dieneri M2
Ns. dieneri M3
Ns. chaohuensis
Ns. aff. cristagalli
Ns. waageni eowaageni
Ns. posterolongatus
Parachirognathus sp.
Ns. n. sp. F
Ns. aff. chaohuensis
Ns. concavus
Ns. n. sp. K
Parachirognathus cf. tricusoidatus
Ns. waageni waageni
Platyvillosus costatus
Ns. n. sp. G
Ns. n. sp. H
Ns. Tongi
Ns. aff. discretus
Pl. hamadai
Ns. peculiaris
Ns. alberti
Claraia hunanica
Claraia greisbachi
Claraia stachei
Claraia radialis
Claraia greisbachi
Claraia aurita
Claraia concentrica
Claraia hubeiensis
Claraia greisbachi
Posidonia minar
Claraia sp.
Guichiella subtotunda
Eumorphotis sp.
Eumorphotis cf. venetina
Eumorphotis huancangenis
Eumorphotis inaequiecostata
Bakevellia costata
Posidonia sp.
Posidonia circularis
Prefl orianites cf. strongi
Arctocer as cf. lolouense
Ophiceras sp.
Lytophicer as? sp.
Prefl orianites? sp.
Arctocer as sp.
Pseudosagecer as sp.
Clypecer as sp.
Owenites pakungensis
Eufl emingites sp.
Konimkites lolowensis
Flemingites ellipticus
Pseudocellites sp.
Prophingitoides sp.
Lytophicer as? sp.
Pseudosagecer as sp.
Flemingites kaoyunlingensis
Ussuria? sp.
Wasachites sp.
Koninckites sp.
Flemingites sp.
Owenites? sp.
Hemiprionites sp.
Eufl emingites cf. tsotengensis
Meekocer as sp.
Juvenites crientalis
Clypeceras cf. lenticulare
Clypecer as cf. kwangsiensis
Dienerocer as sp.
Prionolobus sp.
Dienerocer as diener
Dienerocer as cf. ovale
Pseudosagecer as tsotengsene
Koninckites cf. loloensis
Lithology
Limestone
Nodular limestone
Argillaceous limestone
Mudstone
Claystone
Siliceous mudrock
Conodont Zone
H. typicalis
Ng. krystyni
Ns. kummeli
Ns. dieneri M1
Ns. dieneri M2
Ns. dieneri M3
Ns.dieneri
Ns. waageni eowaageni
Ns. waageni waageni
Neospathodus waageni
Ammonoid Zone
Ophicer as - lyptophicer as
Prionolobus - Gyronites
Flemingites - Eufl emingites
Anasibirites
Bivalve Assemblage Zone
Claraia stachei - C. aurita
Eumorphotis inaequi coastata - E. huancangensis
Guichiella angulata

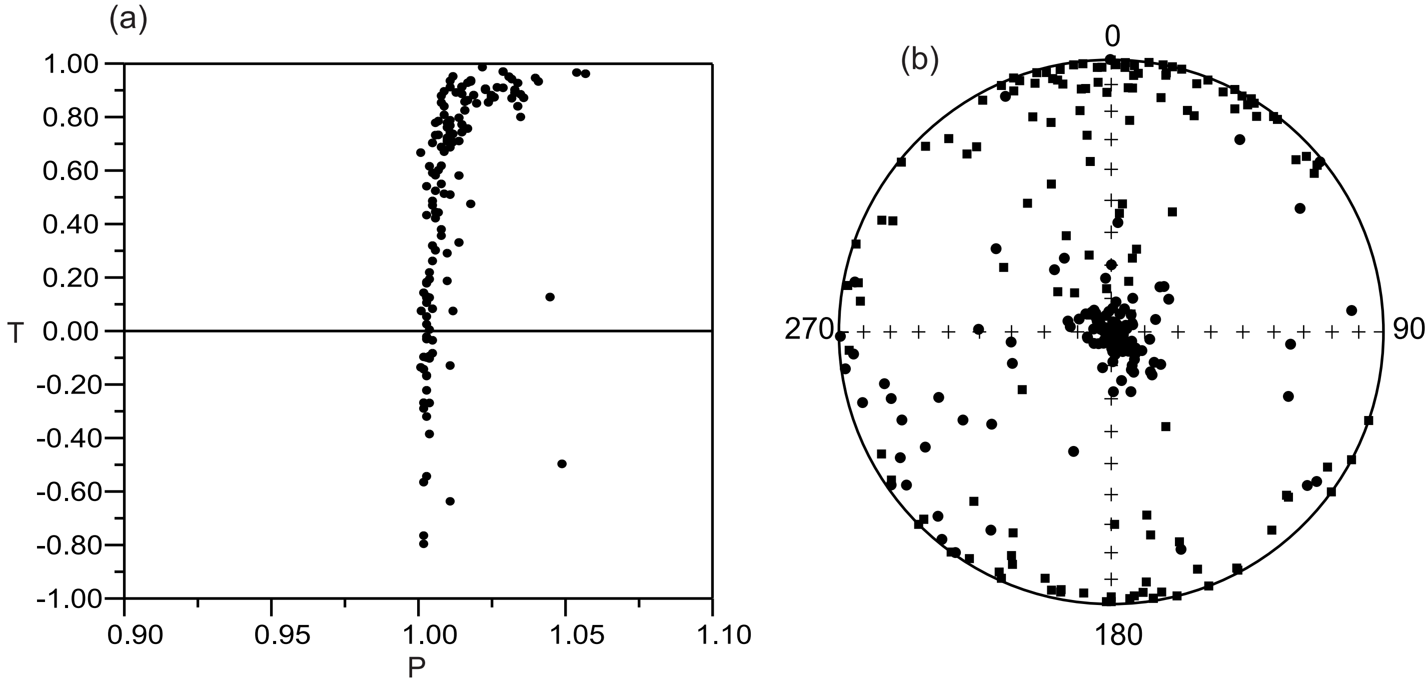
(a)
1.00
0.80
0.60
0.40
0.20
T
0.00
-0.20
-0.40
-0.60
-0.80
-1.00
0.90
0.95
1.00
1.05
1.10
P
(b)
0
270
90
180

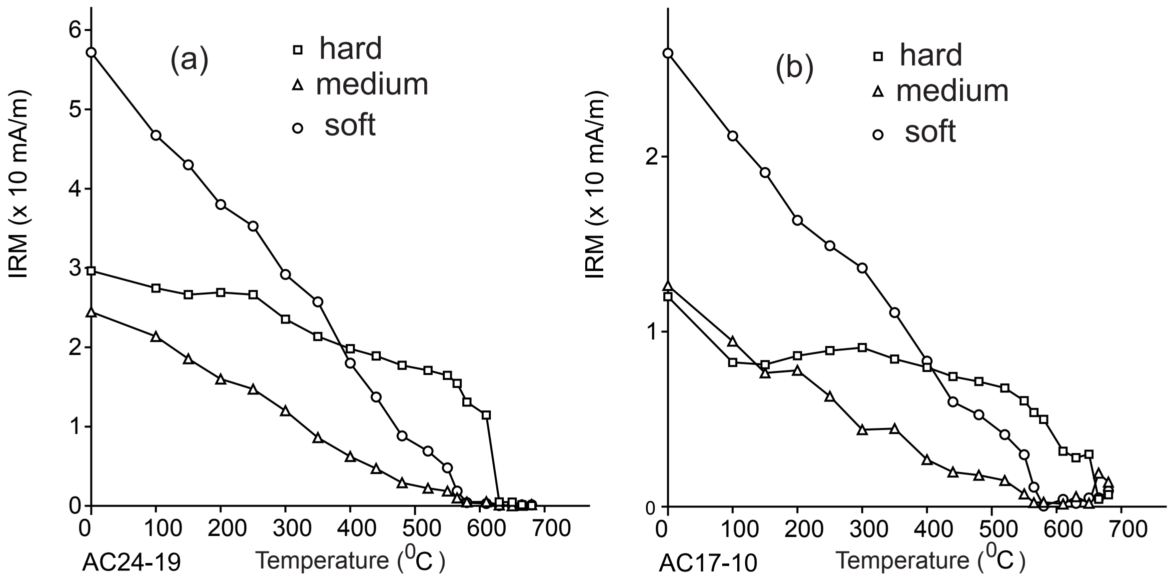

(a)
hard
medium
soft
IRM (x 10 mA/m)
6
5
4
3
2
1
0
0
100
200
300
400
500
600
700
AC24-19
Temperature (0C)
(b)
hard
medium
soft
IRM (x 10 mA/m)
2
1
0
0
100
200
300
400
500
600
700
AC17-10
Temperature (0C)

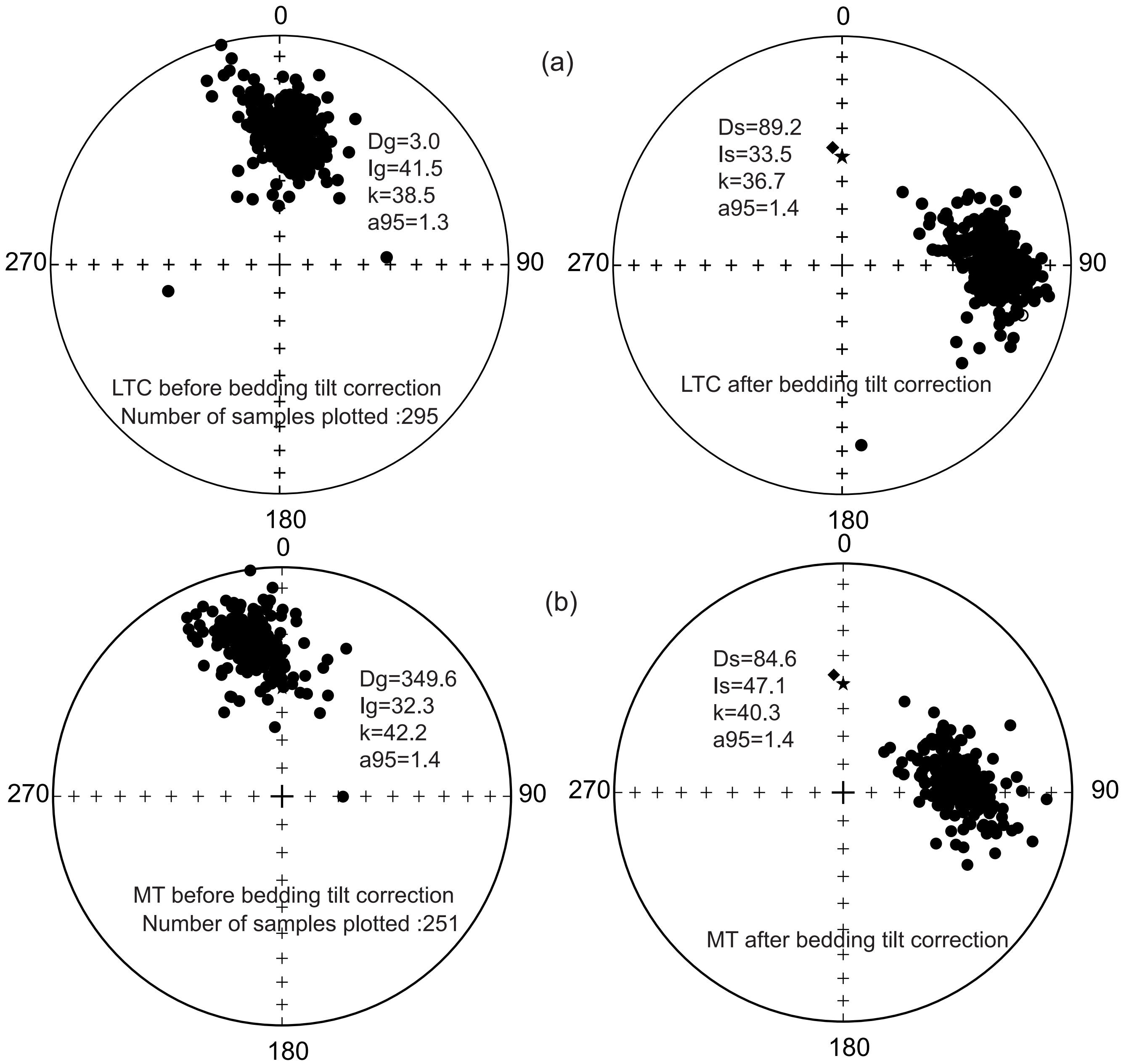
(a)
0
90
180
270
Dg=3.0
Ig=41.5
k=38.5
a95=1.3
LTC before bedding tilt correction
Number of samples plotted :295
Ds=89.2
Is=33.5
k=36.7
a95=1.4
LTC after bedding tilt correction
(b)
Dg=349.6
Ig=32.3
k=42.2
a95=1.4
MT before bedding tilt correction
Number of samples plotted :251
Ds=84.6
Is=47.1
k=40.3
a95=1.4
MT after bedding tilt correction

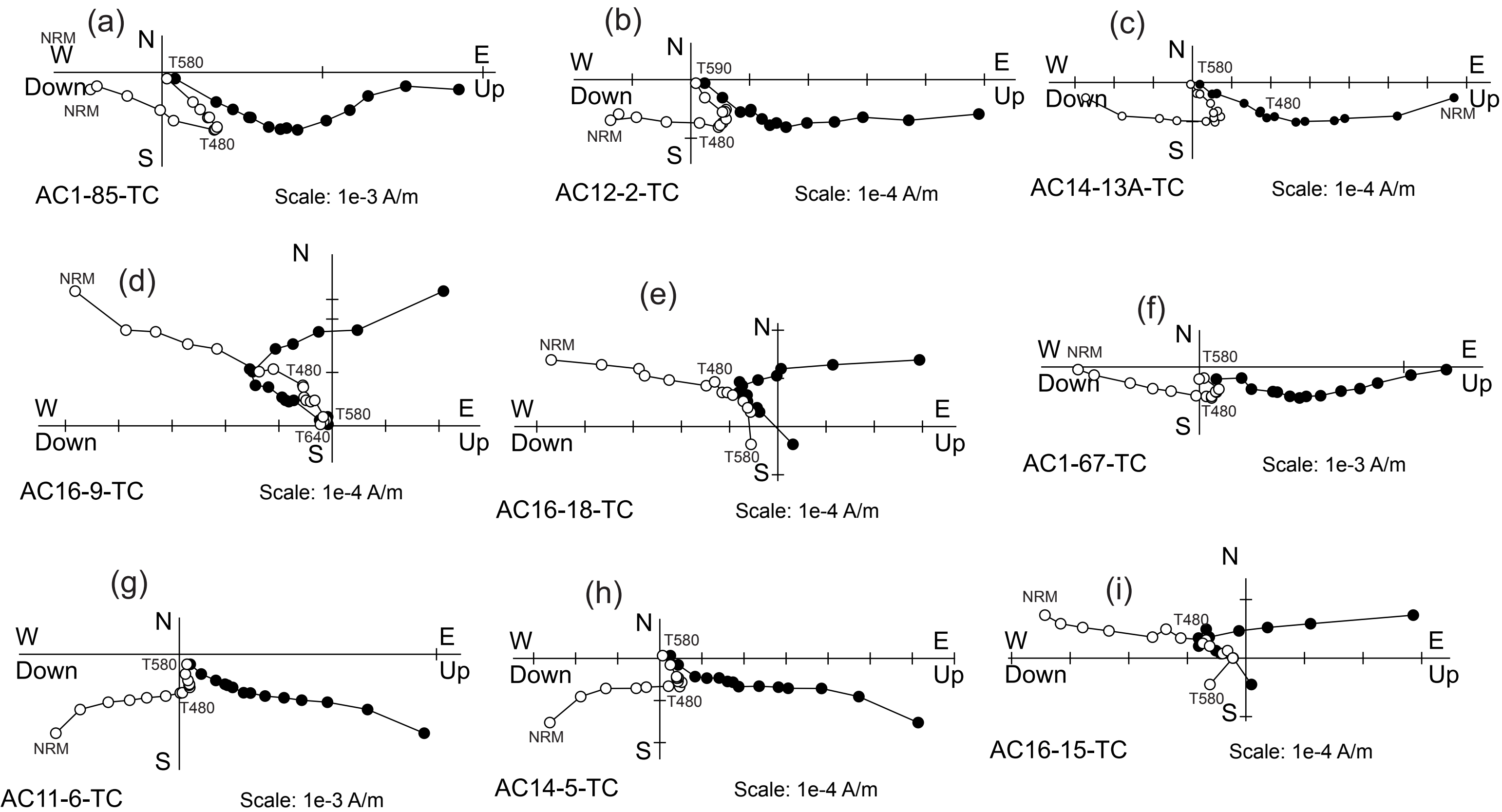
(a)
AC1-85-TC
Scale: 1e-3 A/m
(b)
AC12-2-TC
Scale: 1e-4 A/m
(c)
AC14-13A-TC
Scale: 1e-4 A/m
(d)
AC16-9-TC
Scale: 1e-4 A/m
(e)
AC16-18-TC
Scale: 1e-4 A/m
(f)
AC1-67-TC
Scale: 1e-3 A/m
(g)
AC11-6-TC
Scale: 1e-3 A/m
(h)
AC14-5-TC
Scale: 1e-4 A/m
(i)
AC16-15-TC
Scale: 1e-4 A/m
N
S
W
E
Down
Up
NRM
T480
T580
T590
T640

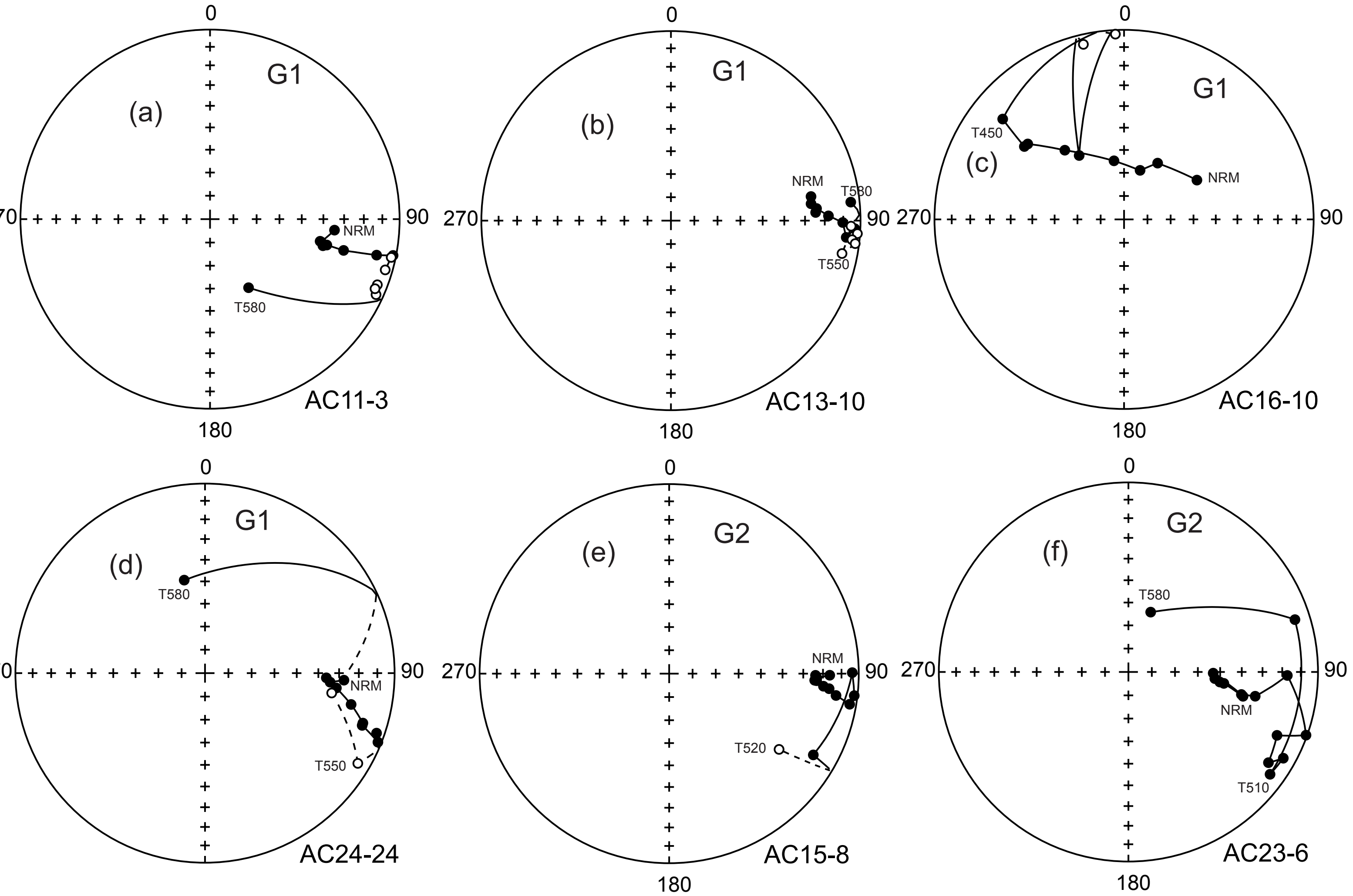

0
90
180
270
G1
(a)
NRM
T580
AC11-3
(b)
T580
T550
AC13-10
(c)
T450
AC16-10
(d)
AC24-24
G2
(e)
T520
AC15-8
(f)
T510
AC23-6

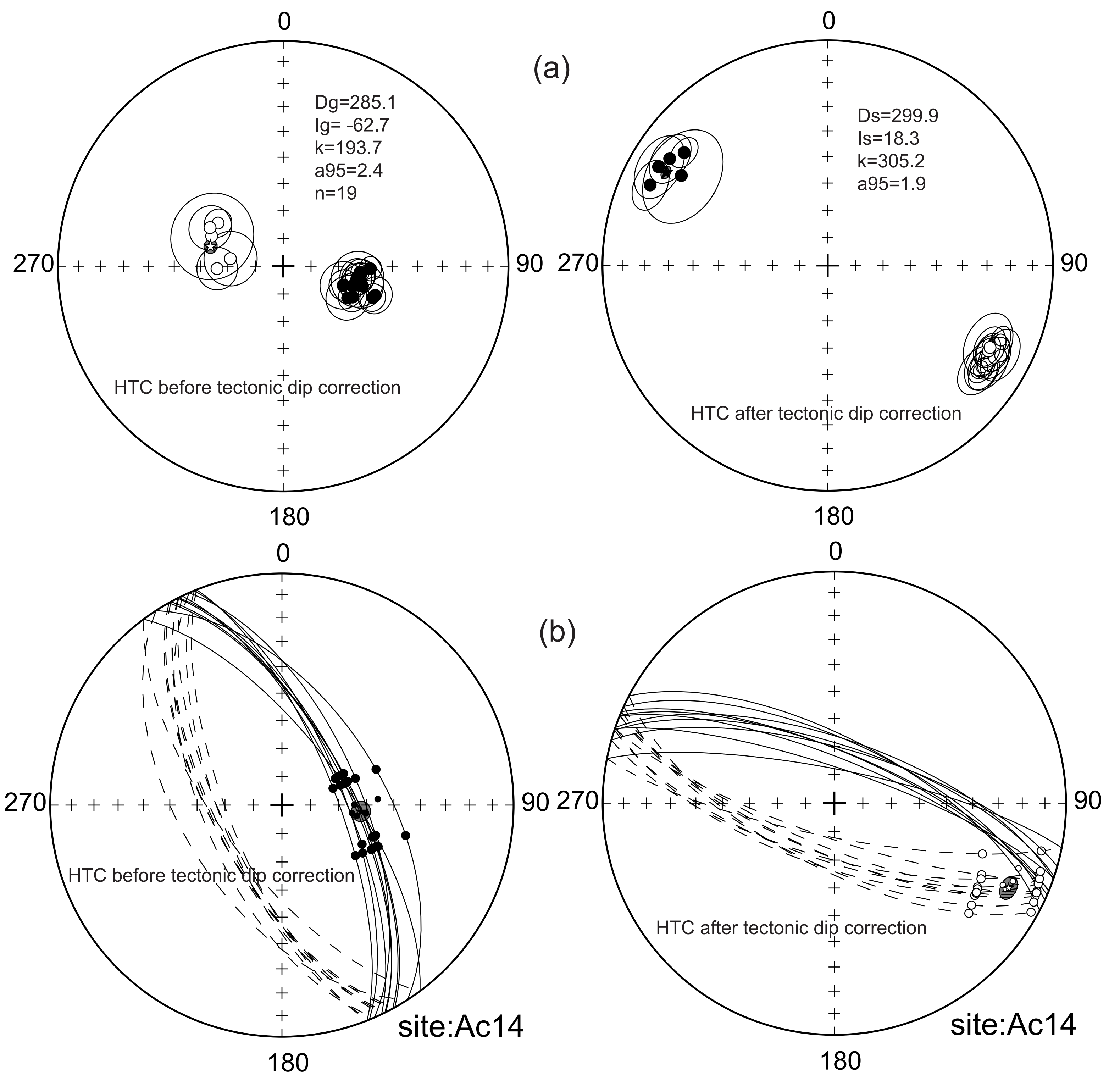
(a)
0
90
180
270
Dg=285.1
Ig= -62.7
k=193.7
a95=2.4
n=19
HTC before tectonic dip correction
Ds=299.9
Is=18.3
k=305.2
a95=1.9
HTC after tectonic dip correction
(b)
HTC before tectonic dip correction
site:Ac14
HTC after tectonic dip correction
site:Ac14

Figure

Click here to download Figure: fig 9.pdf

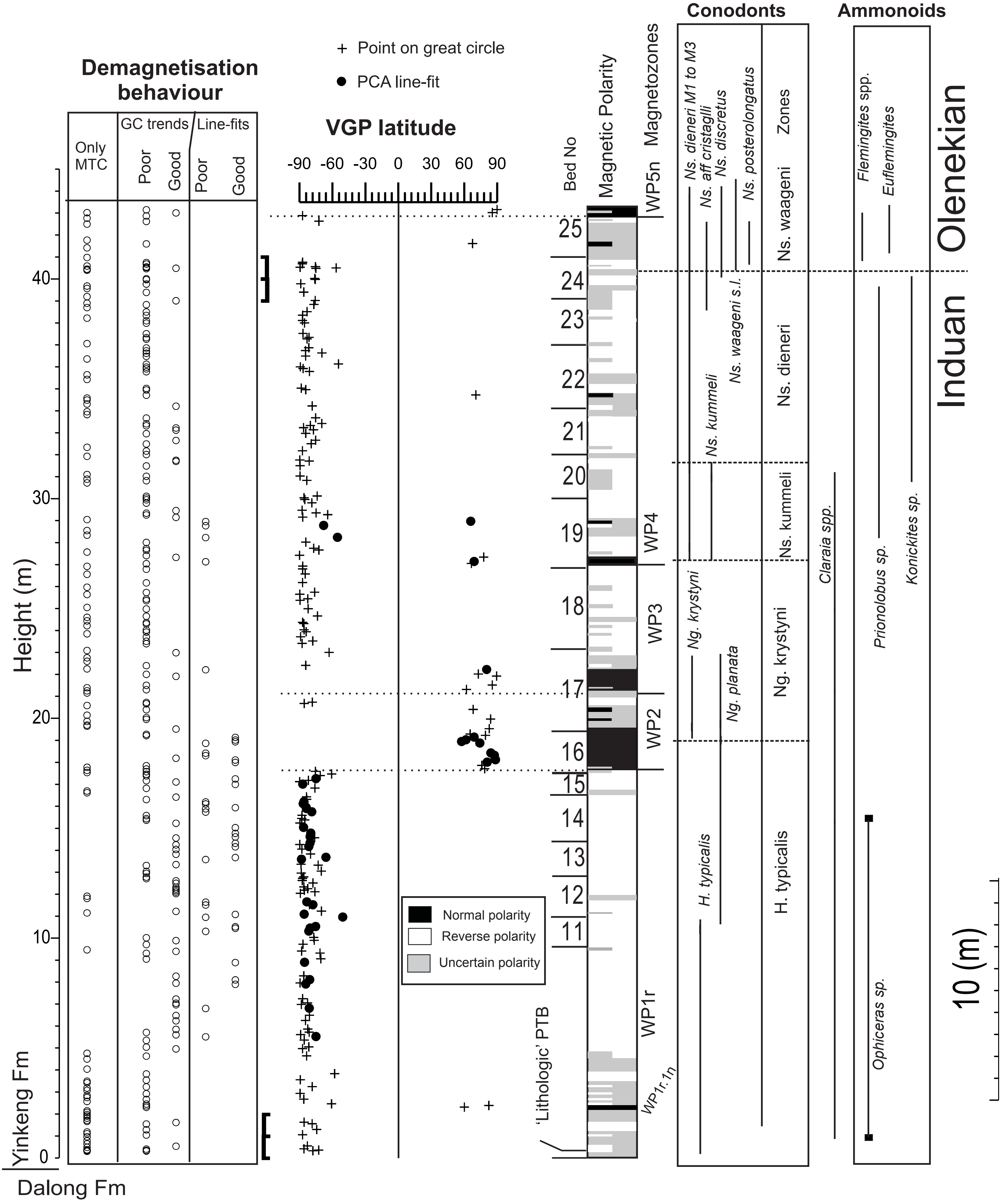

Figure

Click here to download Figure: fig 10.pdf